Marine Pollution Bulletin 215 (2025) 117872

Contents lists available at ScienceDirect

Marine Pollution Bulletin

journal homepage: www.elsevier.com/locate/marpolbul

Evolutionary insights into adaptation of hemocyanins from deep-sea hydrothermal vent shrimps

Hyeongwoo Choi [a,b], Ok-Hwan Yu [c], Seong-il Eyun [a,*]

[a] Department of Life Science, Chung-Ang University, Seoul 06974, Korea
[b] Research Center for Marine-Integrated Biomedical Technology, Pukyong National University, Busan 47122, Korea
[c] Marine Ecosystem and Biological Research Center, Korea Institute of Ocean Science and Technology, Busan 49111, Korea

ARTICLE INFO

Keywords:
Hydrothermal vent
Deep-sea
Alvinocarididae
Adaptation
Hemocyanin
Positive selection

ABSTRACT

Deep-sea hydrothermal vent shrimps inhabit environments with low oxygen levels and may even be exposed to hypoxic conditions. In response, their respiratory pigment, hemocyanin (Hc) may undergo molecular adaptations to enable them to survive in such extreme ecosystems. Therefore, we sampled four Alvinocarididae species from hydrothermal vents in the northern Central Indian Ridge and two types of *Hc* genes (α and γ) were observed. Employing the branch model, we detected positive selection for the deep-sea hydrothermal vent lineage, including 11 Decapoda species. Furthermore, using the branch-site model, we identified a putative mutant residue (Leu226, Ser377, and Ile390) close to the active site of Hc. Moreover, our results suggested potential molecular docking between two α-type Hc proteins. Thus, this study provides valuable and novel perspectives on the functional significance of the *Hc* gene in deep-sea hydrothermal vent shrimps, laying the foundation for future investigations in this intriguing area of research.

1. Introduction

Rising ocean temperature driven by global warming are intensifying oxygen depletion in marine ecosystems. Warmer waters retain less dissolved oxygen, while the metabolic demands of organisms in these habitats increase (Dillon et al., 2010). This phenomenon poses a serious risk to benthic environments, as it may extend the duration of thermocline and contribute to the expansion of hypoxic and anoxic zones in deeper layers of the ocean (Liu et al., 2019). Furthermore, deoxygenation resulting from organic matter decomposition and increased respiration rates further threatens benthic ecosystems as the climate continues to warm (Matear and Hirst, 2003; Bendtsen and Hansen, 2013). As warming continues, benthic animals are forced to adapt to these stressful conditions. However, the molecular mechanisms underlying marine animals' responses to hypoxic environments remain largely unexplored (Wu, 2002).

Deep-sea hydrothermal vents represent dynamic and extreme environments characterized by absence of light, hypoxic conditions, elevated carbon dioxide levels, low PH, high concentrations of heavy metals, and other toxic substances (Van Dover, 2000; Le Layec and Hourdez, 2021). Particularly, organisms that inhabit these habitats are exposed to chronic hypoxia and sometimes complete anoxia (Decelle et al., 2010). In the same context, long-term acclimation of decapods to a hypoxic environment increases the amount of their respiratory pigment, hemocyanin (Hc) (Defur et al., 1990; Mangum, 1994). Therefore, given that oxygen deficiency persists for an extended period in deep-sea hydrothermal vents, respiratory pigments (Hc) in decapods may experience stronger adaptive pressures.

Hc, a respiratory protein in the hemolymph of both mollusks and arthropods, plays a physiologically vital role in these organisms owing to its oxygen transport ability (Markl, 2013). It has a binuclear Cu-active site with three Cu-binding histidine residues (Jaenicke et al., 1999). This type-3 copper center also exists in tyrosinases, catechol oxidases, and phenol oxidases. Thus, the first members of the arthropod Hc superfamily are believed to have evolved from tyrosinase-like ancestral oxygen-binding proteins 600 million years ago (Burmester, 2002). The traditionally recognized function of Hc is oxygen transport. Moreover, in decapods, Hc is involved in other stress responses (Zhang et al., 2009; Sun et al., 2012). For example, the exposure of *Penaeus vannamei*, to ammonia stress results in the significant upregulation of *Hc* which increased antimicrobial activity (Zhao et al., 2022). Additionally, Hc is a multifunctional protein that plays multiple roles in immune defense (Hui et al., 2017; Coates and Costa-Paiva, 2020).

Invertebrates possess multiple Hc subunits that exhibit distinct

* Corresponding author.
E-mail addresses: creo9447@pknu.ac.kr (H. Choi), ohyu@kiost.ac.kr (O.-H. Yu), eyun@cau.ac.kr (S.-i. Eyun).

https://doi.org/10.1016/j.marpolbul.2025.117872
Received 12 March 2024; Received in revised form 22 March 2025; Accepted 22 March 2025

functions. Arthropod Hc is predominantly a hexamer (1 × 6-mer) consisting of six similar heterogeneous or homogeneous subunits, each of which may bind to an oxygen molecule; this hexamer is the predominant form in crustaceans (Sellos et al., 1997). For the deep-sea hydrothermal vent shrimp, *Rimicaris exoculata,* it is reported that their Hc is mostly composed of hexameric (Lallier and Truchot, 1997). This hexamer is more specifically characterized as a "trimmer of dimers" (Van Holde and Miller, 1995). However, even within crustaceans, the quaternary structures of Hc vary; a 2 × 6-mer has been observed in the mantis shrimp, *Squilla mantis* (Hoplocaridae) (Bijlholt and van Bruggen, 1986), while a 4 × 6-mer has been observed in the thalassinid shrimp, *Callianassa californiensis* (Callianassidae) (Miller et al., 1977). Further, linker subunit dimers often hold higher-order Hc oligomers together via ionic or disulfide bonds (Stöcker et al., 1988). Moreover, immunological and molecular phylogenetic studies have shown the existence of three distinct Hc types in Decapods, namely, α, β, and γ Hc (Kusche et al., 2003). These three subtypes were classified based on the immunological cross-reactivity properties (Markl, 1986). These Arthropod *Hc* genes were assumed to be originated 550 million years ago from oxygen-consuming enzymes, phenoloxidases (Burmester, 2004). Phylognetic analysis using molecular clock revealed that the first β-type *Hc* gene diverged from crustacean *Hc* gene approximately 315 million years ago, while the divergence between α- and γ-type *Hc* genes occurred approximately 258 million years ago (Burmester, 2004). Furthermore, seven distinct variants have been identified within the α- and γ-types in crustaceans (Brouwer et al., 1978). However, the relationships between these Hc types remain unclear. Additionally, no evidence of Hc-positive selection in deep-sea hydrothermal vent shrimps has been reported thus far. In addition, a recent study on *Penaeus vannamei* focused to identify the functions of each Hc subtype (Li et al., 2024). While some showed tissue-specific expression, most of the Hc subtypes showed similar function roles. Therefore, detecting natural selection at the amino acid level is of great significance in the field of molecular evolution research. In this study, we collected four alvinocaridids from hydrothermal vents and performed whole-genome sequencing. Among the four deep-sea hydrothermal vent shrimp species, one was identified as a previously unreported species belonging to the family Alvinocarididae. Further, we identified two Hc types (α and γ) in the four deep-sea hydrothermal vent shrimps and resolved their phylogenetic relationships within the order Decapoda. Subsequently, we identified a putative point mutation in *Hc* that may contribute to oxygen affinity. This study sheds light on the adaptation strategies of deep-sea hydrothermal vent shrimps and provides valuable insights into their survival in deep-sea hydrothermal vents.

2. Materials and method

2.1. Sample collection, library construction, and sequencing

In 2019, we collected shrimps (four Alvinocarididae species) from the Onnuri vent field (OVF, 11°14′55.92″ S, 66°15′15.10″ E) at a depth of 2014.5 m using a video-guided hydraulic grab (television grab) carried by the research ship "ISABU", during the KIOST expedition along the Central Indian Ridge. After collection, the specimens were immediately preserved in 95 % ethanol at −80 °C aboard until arrival at the laboratory, where DNA extraction was performed. Specifically, genomic DNA was extracted from the muscle tissues of the shrimps using a Qiagen Blood & Cell Culture DNA Mini Kit according to the manufacturer's instructions.

Library construction was performed with a 550 bp insert using a TruSeq DNA Nano kit. The DNA fragments ligated with an adaptor were amplified via PCR. Thereafter, the resulting DNA fragments were selected and subjected to paired-end sequencing using the Illumina NovaSeq 6000 platform.

2.2. Data filtering and genome assembly

Before genome assembly, adapter sequences, low-quality reads (Phred quality score < 20) and reads shorter than 120 bp or reads with Ns were filtered using trim_galore (ver. 0.6.6) with the parameter "–quality 20 –length 120 –max_n 0" (Martin, 2011). De novo genome assembly was performed using SPAdes (ver. 3.14.0), a universal *de Brujin* assembler that uses k-mers (k-mers 21, 31, 51, 71, 91, and 121 were used in this study) to build the initial *de Bruijn* graph (Bankevich et al., 2012; Jung et al., 2020; Choi et al., 2024, 2025). For genome assessment, busco (ver. 5.4.3) was employed based on the metazoan_odb10 dataset (Simão et al., 2015). Furthermore, to obtain diverse metrics, such as the number of contigs, the largest contig, total length, N50, and L50, without a reference genome, we used QUAST (ver. 5.0.2), a quality assessment software for genome assembly (Gurevich et al., 2013). The mitochondrial genome was assembled using MITOZ software (ver. 3.6) (Meng et al., 2019) and visualized using Circos (ver. 0.69-8) (Krzywinski et al., 2009). To identify protein-coding genes, we performed ab initio gene prediction using augustus (ver. 3.4.0) with the parameter "–species = notospermus_geniculatus" (Stanke and Morgenstern, 2005).

2.3. Hc gene prediction and annotation

To extract *Hc* genes from the four Alvinocarididae shrimps included in this study, we created a custom database consisting of the three Hc types (α, β, and γ) and pseudo-hemocyanin (Supplementary Table S1). Thereafter, we performed blastp searches to compare protein queries to our custom BLAST database using the following parameters: cutoff e-value, 0.0; length, 350 aa; and identity cutoff, 60 %. We predicted the domains for each gene using a Simple Modular Architecture Research Tool (SMART) (Schultz et al., 2000). We further extracted the putative *Hc* genes from those containing at least two of the three domains: hemocyanin_N, hemocyanin_M, and hemocyanin_C.

2.4. Phylogenetic analysis

Three phylogenetic analyses were performed. These included Alvinocarididae species tree analysis using mitochondrial 13 protein-coding genes (PCGs), Decapoda gene tree analysis using the *Hc* gene, and Decapoda species tree analysis using the cytochrome *c* oxidase subunit 1 (*COX1*).

To construct the Alvinocarididae species tree, mitochondrial DNA from 15 caridean species, including 11 species obtained from the National Center for Biotechnology Information (NCBI, https://www.ncbi.nlm.nih.gov) and the four deep-sea hydrothermal vent shrimps collected in this study were used. For the outgroup species, *Pandaulus hypsinotus* was used. The nucleotide sequences of 13 PCGs were also extracted from the mitochondrial genomes. Further, multiple sequence alignment (MSA) was separately performed for each gene using mafft (ver. 7.505) (Katoh et al., 2002), while PartitionFinder2 (Lanfear et al., 2016) was used to determine the best-fit substitution model for each gene set based on the Bayesian information criterion (BIC). Finally, the aligned PCGs were concatenated for phylogenetic analyses.

To construct the Decapoda gene tree, 33 published Hc amino acid sequences were obtained from the NCBI and used along with 15 *Hc* sequences obtained in this study. The Hc amino acid sequences were aligned using mafft. Further, phylogenetic relationships between Hc types (α, β, and γ) were resolved using maximum likelihood (ML) and Bayesian Inference (BI) models. Then, to determine the best-fit evolutionary substitution model for each Hc type based on the BIC, ModelFinder (Kalyaanamoorthy et al., 2017) in IQ-Tree2 (ver. 2.2.0.3) (Minh et al., 2020) was used.

To construct the Decapoda species tree, *COX1* sequences from 11 Decapoda species and one Amphipoda species were used. The decapod species tree thus obtained was then used as an input tree file for the

Table 1
Summary of next-generation sequencing to genome annotation for four deep-sea hydrothermal vent shrimps. Abbreviations: C, complete Benchmarking Universal Single-Copy Orthologues (BUSCOs); S, single-copy BUSCOs; D, duplicated BUSCOs; F, fragmented BUSCOs; M, missing BUSCOs.

		Rimicaris kairei	*Rimicaris* cf. *variabilis*	*Alvinocaris longirostris*	Alvinocaridid sp.
Sequencing	Platform	Illumina Novaseq6000	Illumina Novaseq6000	Illumina Novaseq6000	Illumina Novaseq6000
	Library kit	TruSeq DNA Nano 550 bp	TruSeq DNA Nano 550 bp	TruSeq DNA Nano 550 bp	TruSeq DNA Nano 550 bp
	Read length (bp)	151 × 2	151 × 2	151 × 2	151 × 2
	Insert size (bp)	550	550	550	550
	Number of reads	197,343,290	201,371,554	228,077,610	260,426,508
	Mean quality score	33.32	33.40	33.84	34.74
	Percentage of ≥Q30 (%)	79.38	79.78	83.66	86.79
	Number of bases (Gb)	29.80	30.41	34.44	39.32
Data filtering	Number of reads	190,642,324	163,911,744	196,635,812	241,241,848
	Number of bases (Gb)	24.01	24.47	29.40	36.16
Assembly (>1000 bp)	Number of contigs	296,082	303,039	483,219	639,218
	Length of N50 (bp)	1426	1392	1767	1937
	Total length of contigs (Mb)	442.40	438.25	843.07	1195.52
	Largest contig (Kb)	77.61	79.18	36.85	55.94
	GC content (%)	34.99	34.56	34.84	34.81
	BUSCO result (C, [S, D], F, M) (%)	13, [8.8, 4.2], 40.4, 46.6	9.9, [8.5, 1.4], 43.9, 46.2	11.1, [10.9, 0.2], 48.6, 40.3	17.1, [15.5, 1.6], 48, 34.9
Gene prediction	Number of predicted genes	101,595	120,529	164,904	212,914

positive selection analysis.

ML and BI phylogenetic trees were constructed using raxml-ng (ver. 1.1.0) (Kozlov et al., 2019) and MrBayes (ver. 3.2.6) (Ronquist et al., 2012), respectively. For the evaluation of the tree topologies, 1000 non-parametric bootstrap replicates were employed in the ML analysis. Further, in the BI analysis, Bayesian posterior probabilities (BPP) were calculated using four independent Markov Chain Monte Carlo (MCMC) runs, each consisting of 1.0×10^6 generations. Samples were obtained every 500th generation, with the initial 25 % of the data discarded as burn-ins. The tree topology from the ML analysis was visualized using FigTree (ver. 1.4.4.) (http://tree.bio.ed.ac.uk/software/figtree).

2.5. Determination and visualization of positively selected genes

To clarify the genomic adaptation mechanisms of Hc in shrimps inhabiting deep-sea hydrothermal vent environments, we utilized the codeml program in the PAML (Phylogenetic Analysis by Maximum Likelihood) package (ver. 4.10.5) (Yang, 2007) to identify positively selected genes. The Decapoda species tree obtained using raxml-ng was used as the input tree file, after which it was unrooted, and its branch lengths were removed. In addition, we treated the deep-sea hydrothermal vent lineage as a polytomy. The aligned amino acid sequences obtained from MAFFT were used to align the DNA sequences using pal2nal (ver. 14) (Suyama et al., 2006). For the selection analysis, we employed branch and branch-site models.

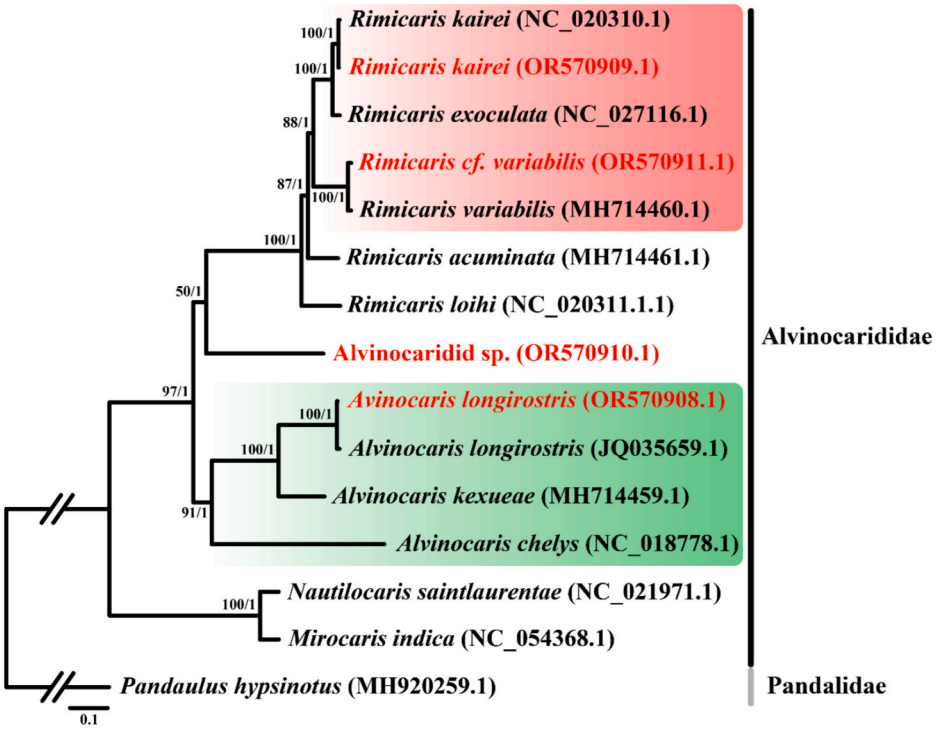

Fig. 1. Maximum likelihood phylogenetic species tree obtained based on 13 concatenated mitochondrial protein-coding genes inferred from 15 caridean species. *Pandalus hypsinotus* was used as the outgroup species. The bootstrap values (left) and Bayesian poster probability values (right) are labeled at each node. The names in red represent the deep-sea hydrothermal vent shrimp samples considered in this study. The clades highlighted with red and green backgrounds correspond to the genera *Rimicaris* and *Alvinocaris*, respectively.

In the branch model, we compared a null model (model = 0, NSsites = 0), assuming an equal d_N/d_S ratio across all clades, with an alternative model (model = 2, NSsites = 0), allowing for different d_N/d_S ratios in the foreground branch (representing the deep-sea hydrothermal vent chemosynthetic environment), unlike the background branch. Likelihood ratio tests (LRT) and chi-square (χ^2) distributions were used to determine the best-fit models and assess the statistical significance of the *p*-values obtained. In cases where the LRT was statistically significant ($p < 0.1$) and the ω (d_N/d_S) ratio was >1, the site was considered to be under positive selection.

For the branch-site model, we compared a null model (model = 2, NSsites = 2, fix_omega = 1) with an alternative model (model = 2, NSsites = 2, fix_omega = 0), allowing the d_N/d_S ratio to vary among the codon sites. A positively selected site was identified when the Bayes Empirical Bayes (BEB) value was >95 % and the *P*-value was <0.05.

AlphaFold2 (ver. 2.3.1) (Jumper et al., 2021) was used to predict the three-dimensional (3D) structures of Hc in the deep-sea hydrothermal vent shrimps. Molecular docking of Hcs was predicted using ClusPro 2.0 (https://cluspro.org) (Kozakov et al., 2017) and visualized using PyMOL (ver. 4.6) (Schrödinger and DeLano, 2020).

2.6. Detection of convergence amino acid substitution

To investigate amino acid convergence within the deep-sea hydrothermal vent lineage, we utilized a dataset containing orthologous α-type *Hc* amino acid sequences from 12 Malacostraca species. Phylogenetic tree reconstruction and the inference of ancestral Hc amino acid were performed by RAxML. Subsequently, Seq-Gen (ver. 1.3.4) (Rambaut and Grass, 1997) was employed to conduct 100,000 Monte-Carlo simulations of amino acid sequence evolution along the phylogenetic tree, employing the "WAG" substitution model. The simulated dataset was then analyzed to detect amino acid replacements occurred by random chance.

3. Results

3.1. Genome characteristics and gene annotation

Raw reads ranging from 29 to 39 Gb were generated via whole-genome sequencing on samples corresponding to four deep-sea hydrothermal vent shrimp species collected from a hydrothermal vent on the Illumina NovaSeq 6000 platform (Table 1). After data filtering, filtered reads in the 24–36 Gb range were obtained for the four samples. The number of contigs in our assembled data was below 639,218, with the GC content ranging from 34.56 to 34.99 %. Moreover, we obtained >101,595 protein-coding genes from the genome of four deep-sea hydrothermal vent shrimp species. Table 1 provides more details regarding each assembly result at the contig level and the gene annotation results.

3.2. Species identification

For species identification using each sample, we performed BLAST searches using the *COX1* gene. The identity values of three shrimp species exceeded 98.7 %, leading to the adoption of the best-matching species as the sample names (Supplementary Table S2). For one sample, the identity value was 88.5 %, which is inadequate for species identification at the species level. Therefore, this particular species was assigned the name "Alvinocaridid sp.". Next, we used 13 mitochondrial PCGs to reveal the phylogenetic relationships among the four deep-sea hydrothermal vent shrimp species. Based on the phylogenetic analysis, the four deep-sea hydrothermal vent shrimp species were placed within the family Alvinocarididae (Fig. 1).

3.3. Hc gene identification and phylogenetic analysis

To extract *Hc* genes from the genomes of the four deep-sea hydrothermal vent shrimp species collected in this study, we conducted sequence similarity searches using *Hc* genes isolated from *Atyopsis moluccensis* and *Metacarcinus magister* as queries (Supplementary Table S1). Our investigation revealed that Alvinocarididae shrimps possess α- and γ-type *Hc* and showed the absence of β-type *Hc* and pseudo-*Hc* in their genome (Table 2).

Table 2
BLAST results for hemocyanin genes obtained from four Alvinocarididae shrimps.

Sample name	Top gene	Length (bp)	Gene name	Identified group	Accession number
Rimicaris kairei	g629.t1	659	*RkaHc1*	α	OR515028
	g1631.t1	498	*RkaHc2*	γ	OR515029
	g3294.t1	497	*RkaHc3*		OR515030
Rimicaris cf. *variabilis*	g1120.t1	659	*RvaHc1*	α	OR515025
	g7496.t1	358	*RvaHc2*	γ	OR515026
	g1530.t1	498	*RvaHc3*		OR515027
Alvinocaris longirostris	g3831.t1	624	*AloHc1*	α	OR515021
	g950.t1	498	*AloHc2*	γ	OR515022
	g8878.t1	357	*AloHc3*		OR515023
	g10250.t1	497	*AloHc4*		OR515024
Alvinocaridid sp.	g6568.t1	513	*AspHc1*	α	OR515031
	g25027.t1	654	*AspHc2*	γ	OR515032
	g1532.t1	498	*AspHc3*		OR515033
	g4055.t1	498	*AspHc4*		OR515034
	g11773.t1	497	*AspHc5*		OR515035

An ML tree was constructed using the 48 amino acid sequences of Hc (Fig. 2). Three genes isolated from Insecta species were used as outgroups. In the ML gene tree, the α-type *Hc* of the deep-sea hydrothermal vent lineage exhibited monophyly with robust support (BB = 100 and BPP = 1). However, the node supportive values for γ-type *Hc* were relatively low (BB = 54 and BPP = 0.8). Further, we identified multiple paralogues of γ-type *Hc* within the deep-sea hydrothermal vent shrimp species, in contrast to what was observed for α-type *Hc* (a single copy gene). The number of gene copies ranged from two to four, demonstrating inconsistency across species. However, since all γ-type *Hc* paralogues originated from distinct contigs, these additional gene copies likely stemmed from gene duplication events rather than mere isoform variations.

3.4. Detecting positive selection under deep-sea hydrothermal vent adaptation

As phylogenetically distant taxa could potentially lead to undue influence on selection analysis, we constructed a new species tree comprising 12 Malacostraca species (Supplementary Fig. S1). Thereafter, we investigated two *Hc* types (α and γ) within Alvinocarididae. When the deep-sea hydrothermal vent lineage was used as the foreground branch, both α- and γ-type *Hc* were positively selected by the branch model (Table 3). Notably, the ω (d_n/d_s) ratio on the foreground branch was two-fold as high as that on the background branch.

Given the deep-sea hydrothermal vent lineages experience strong adaptive pressure, we further examined whether any of the sites were positively selected. The results obtained based on the branch-site model revealed significant fitting for the alternative model only for α-type *Hc*

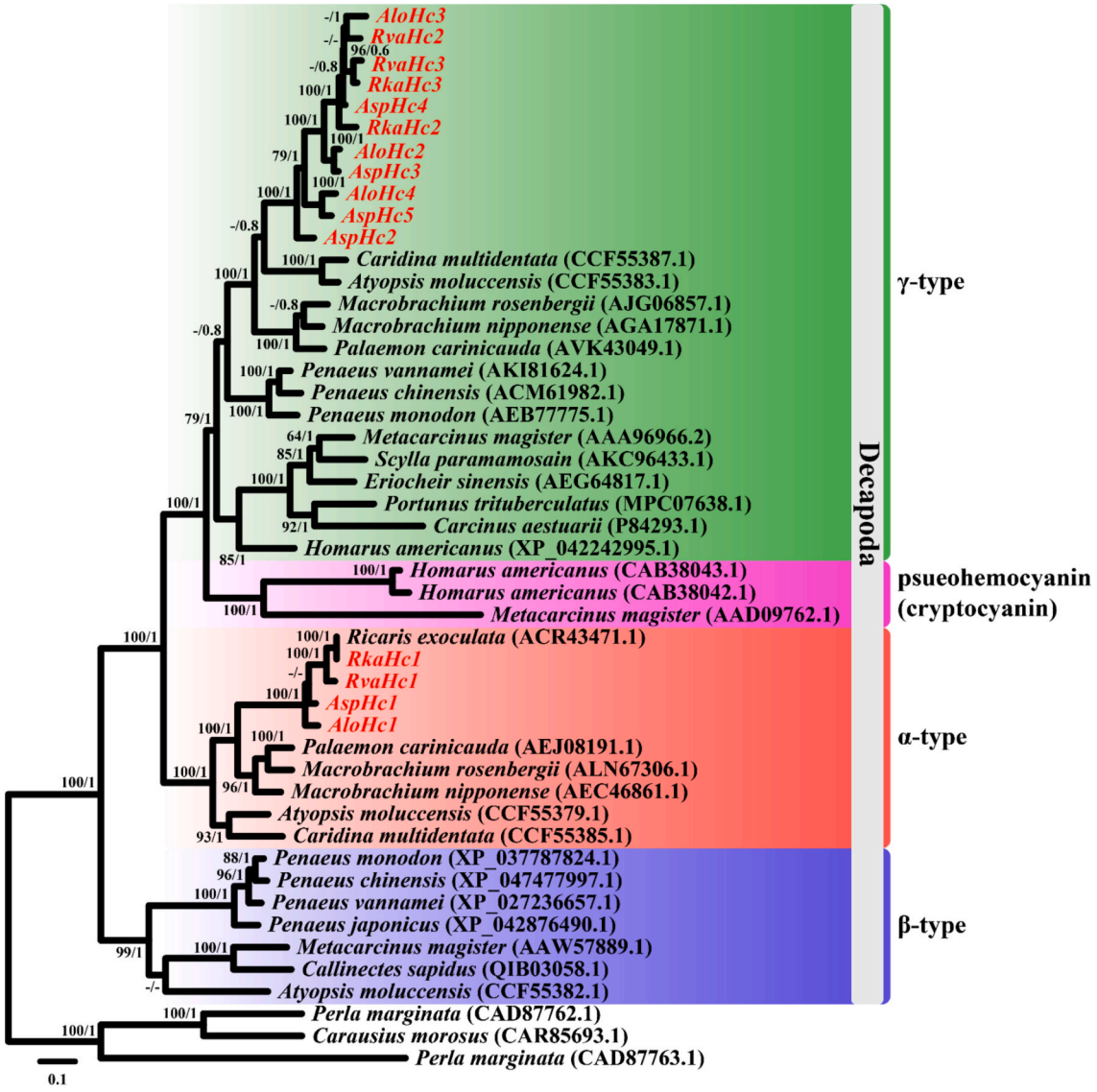

Fig. 2. Maximum likelihood (ML) phylogenetic gene tree based on 48 amino acid sequences of hemocyanin (Hc). Three Insecta species were used as the outgroup. The bootstrap values (left) and Bayesian posterior probability values (right) are labeled at each node. Only support values higher than 60 % and 0.6 inferred from ML and Bayesian Inference, respectively, are shown on each branch. Hc obtained from deep-sea hydrothermal vent shrimps are shown in red. The clades highlighted with green, pink, red, and blue backgrounds correspond to the four types of Hc.

Table 3
Summary of the branch model. Abbreviations: np, number of the parameter; LRT, likelihood ratio test.

Branch	Type	Null model (np)		Alternative model (np)			LRTs	*p*-Value
		−ln L	ω	−ln L	Foreground ω	Background ω		
Deep-sea hydrothermal vent clade	α	−10,555.811223 (23)	0.1217	−10,538.803007 (24)	0.2540	0.1027	34.02	5.45−e9
	γ	−7022.475553 (23)	0.0869	−7016.889049 (24)	0.1572	0.0765	11.17	0.00083

($p < 0.1$) and showed a higher ω ratio (ω = 1.74) for the deep-sea hydrothermal vent lineage (Table 4). Conversely, for α-type *Hc*, 28 positively selected sites were identified. Nine sites were identified as suspected sites according to the BEB values obtained. Among the 28 putatively selected sites, three residues (Leu 226, Ser 377, and Ile 390) were located within the active site of Hc, where six histidine residues bound to copper to enable oxygen transport (Fig. 3a and b).

Our study also revealed the molecular docking of two Hc proteins, resulting in the formation of a homomeric complex (Fig. 4a). Residue 617, which underwent positive selection as identified based on BEB values ($p < 0.01$), was detected within the binding site of the dimer and Hemocyanin_C domain (Fig. 4b and c and Table 4).

3.5. Convergent evolution of Hc in the deep-sea hydrothermal vent shrimps

Since the same amino acid substitutions were observed at positively selected sites in four deep-sea hydrothermal vent shrimps, we tested whether these substitution were the result of convergent evolution. A total of 20,491 simulations were conducted, where two α-type *HC* genes from deep-sea hydrothermal vent shrimp exhibited the same substitution at the same position among 100,000 simulations. However, no cases

Table 4
Summary of the branch-site model. Abbreviations: np, number of the parameter; LRT, likelihood ratio test; BEB, Bayes Empirical Bayes.

Branch	Type	Null model (np)	Alternative model (np)	LRTs (*p*-value)	Site class	0	1	2a	2b
Deep-sea hydrothermal vent claded	α	−110,349.363440 (23)	−10,347.674635 (24)	3.38 (0.066)	Proportion	0.72	0.19	0.08	0.02
					Foreground ω	0.07	1	1.74	1.74
					Background ω	0.07	1	0.07	1
		Positively selected sites (BEB)	149 A (0.620), 173 H (0.961)*, 216 I (0.828), 226 L (0.829), 244 D (0.995)**, 252 N (0.881), 267 F (0.965)*, 289 I (0.942), 294 V (0.959)*, 340 F (0.530), 341 Q (0.543), 352 M (0.760), 358 G (0.967)*, 367 S (0.965)*, 377 S (0.971)*, 390 I (0.532), 412 S (0.865), 414 I (0.566), 428 F (0.733), 485 M (0.929), 556 F (0.950)*, 558 M (0.656), 562 G (0.819), 572 L (0.503), 587 V (0.812), 617 Y (1.000)**, 627 Y (0.880), 658 E (0.922)					
	γ	−6919.140362 (23)	−6917.958407 (24)	2.36 (0.124)	Proportion	0.83	0.12	0.04	0.01
					Foreground ω	0.06	1	2.02	2.02
					Background ω	0.06	1	0.06	1
		Positively selected sites (BEB)	3 Q (0.833), 16 A (0.611), 52 S (0.546), 81 N (0.682), 92 Q (0.984)*, 118 I (0.642), 127 N (0.980)*, 301 P (0.974)*, 305 V (0.630), 327 T (0.573), 344 H (0.656), 354 L (0.805)						

were observed where three or four α-type *HC* genes exhibited the same amino acid substitution (Supplementary Table S3).

4. Discussion

In this study, we performed whole-genome sequencing and bioinformatics analysis and successfully elucidated the intricate evolutionary relationships among four deep-sea hydrothermal vent shrimp species belonging to the family Alvinocarididae collected from hydrothermal vents. Our results provide robust support for the nodes of the three shrimp species (*Rimicaris kairei*, *Rimicaris* cf. *variabilis*, and *Alvinocaris longirostris*) in both bootstrapping replicate (BP = 100) and BPP = 1 analyses (Fig. 1). However, Alvinocaridid sp. was poorly saturated (BP = 50). This finding could be attributed to the lack of mitochondrial genome data for this deep-sea hydrothermal vent shrimp species, which limited the accurate identification of its phylogenetic position. Therefore, additional mitochondrial genomes are required to determine phylogenetic relationships within Alvinocarididae.

Although our assembled genome may not be suitable for whole genome analysis (BUSCO <17.1 % and N50 < 1937), the assembly and annotation of *Hc* genes proceeded without any issues in this study. Additionally, stringent filtering criteria were applied during the extraction of putative *Hc* genes (as detailed in Materials and Method). As a result, we report the presence of two *Hc* gene types (α and γ) in deep-sea hydrothermal vent shrimps for the first time (see Fig. 2 and Table 2 for the *Hc* gene abbreviations). While α-type *Hc* is present in all decapods, the β- and γ-types are absent in several species (Todorovska et al., 2021). A single copy of the α-type *Hc* was observed in each shrimp species, whereas several copies of γ-type *Hc* were observed in each species. Burmester delineated two clades in crustacean Hc types (α and γ), while β-type *Hc* remained unidentified (Burmester, 2001). Additionally, α- and γ-type *Hc* genes are expanded in the genome of *Penaeus* compare to the γ-type *Hc* (Li et al., 2024). This finding is consistent with our observation that none of the four deep-sea hydrothermal vent shrimp possessed β-type *Hc*. However, chromosome-level genome analysis in further study is needed to verify the absence of β-type *Hc* gene in the genome of deep-sea hydrothermal vent shrimps. The α-type *Hc* of the deep-sea hydrothermal vent shrimp species exhibited similar lengths, ranging from 513 to 659 aa, when compared with those of the two lobsters (657 and 660 aa) (Bak et al., 1986; Burmester, 1999) and two shrimp species (641 and 648 aa) (Sellos et al., 1997; Jiewkok et al., 2015). In contrast, γ-type *Hc* exhibited fragmentation, with lengths ranging from 357 to 654 aa (Table 2). Considering that we employed a filtering criterion to exclude genes shorter than 350 aa, there could potentially exist additional gene copies of γ-type *Hc* within the genome of deep-sea hydrothermal vent shrimps. Therefore, further studies employing long-read sequencing are necessary to obtain the full length of γ-type *Hc*. Such studies will provide a comprehensive understanding of the gene duplication phenomenon within populations of deep-sea hydrothermal vent shrimps.

The exposure of deep-sea hydrothermal vent animals to chronic hypoxia (Hourdez and Lallier, 2007) may impose selection pressure on their respiratory pigment, Hc. The oxygen consumption rates of deep-sea hydrothermal vent animals are similar to those of shallow-water species (Hourdez et al., 2002; Hourdez and Weber, 2005), suggesting that these deep-sea hydrothermal vent species have successfully adapted to oxygen-deficient environments. Therefore, we focused on the signs of molecular adaptation (positive selection) in response to deep-sea hydrothermal vent environments. Since most amino acids are expected to undergo purifying selection to eliminate deleterious mutations (Liang et al., 2006), we suspected that 28 residues possibly undergo selection pressure. Consequently, we examined their locations in the 3D structure of α-type *Hc* (Fig. 3a and b). These residues were also found to be located within the Hemocyanin_M domain. Aweya et al. (2022) reported that the armadillo (ARM) repeat within this Hemocyanin_M domain plays a crucial role in antimicrobial responses by activating the p38 MAPK signaling pathway (Fig. 3c) (Aweya et al., 2022). In this study, we identified two positively selected residues (Ser377 and Ile390) located in close proximity to the ARM repeat. Further investigation is needed to elucidate their functional role in enhancing antimicrobial responses. Such domains contribute to the overall function of a protein by performing specific functions or interactions and are evolutionarily conserved (Fong and Marchler-Bauer, 2008). Furthermore, because mutations in these domains can lead to protein distortion (Pal et al., 2020), these positively selected residues can potentially affect the overall structure or stability of Hc. All four deep-sea hydrothermal vent shrimp species showed the same nucleotide substitution in the relatively conserved motif region (Leu226 and Ile390) (Fig. 3d) and these substitutions were exclusively observed in the deep-sea hydrothermal vent clades. Interestingly, among the three positively selected sites, two residues (Leu226 and Ile390) exhibited the same mutation, an occurrence that is exceptionally rare (Supplementary Table S3). Therefore, genomic convergence driven by positive selection may play a pivotal role in the adaptation of deep-sea hydrothermal vent shrimp to extreme environments. In contrast, the γ-type *Hc* does not exhibit statistically significant support for positive selection. This finding implied that γ-type *Hc* might experiences stronger evolutionary constraints than α-type *Hc* and is conserved throughout the evolution of decapods.

Moreover, various intermediate forms, encompassing structures from monomers to hexamers, may also exist (Van Holde and Miller, 1995). Reportedly, mutations can change the binding energy of a dimer by modifying protein interaction kinetics (Zhao et al., 2015). Therefore, positively selected residues can potentially alter the strength of the binding affinity between dimers. Specifically, the substitution of a negatively charged amino acid (Glu) with a hydrophobic (Tyr) or positively charged (His) amino acid can affect the interactions of Hc (Fig. 4d). Therefore, further studies with a focus on the functional properties of Hc dimers, including protein structural stability and

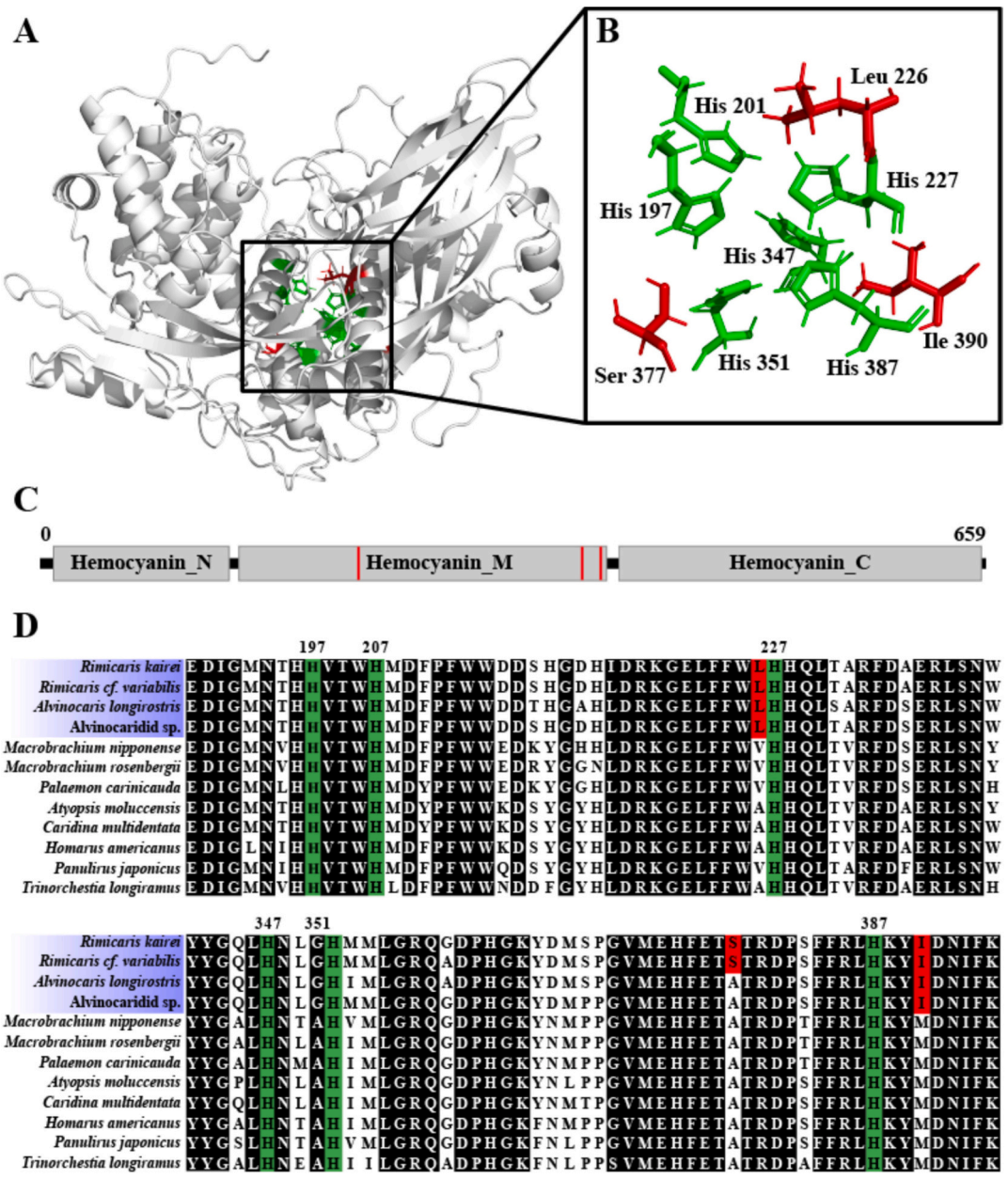

Fig. 3. (a) White ribbon diagram showing the three-dimensional structure of *Rimicaris kairei* α-type hemocyanin (Hc) (*RkaHc1*). The red (three) and green (six) residues represent positively selected and histidine residues within the active site, respectively. (b) Detailed interactions within the active site: three positively selected residues (red) and six histidine residues (green). Three mutations (Leucine, Serine, and Isoleucine) can be observed in close proximity to the active site. (c) Schematic representation of the domains of *RkaHc1*: Hemocyanin_N, Hemocyanin_M, and Hemocyanin_C. The three positively selected residues (red) detected in close proximity to the active site can be observed to be located in the Hemocyanin_M domain. (d) Multiple sequence alignment (MSA) of the Hemocyanin_M domains from 12 decapods. The four deep-sea hydrothermal vent shrimps considered in this study are indicated in blue on the left side of the MSA. Within the alignment, the green background represents six histidine residues, while the red background represents three mutation residues. The black background represents highly conserved regions. Accession numbers: *Macrobrachium nipponense*, AEC46861.1; *Macrobrachium rosenbergii*, ALN67306.1; *Palaemon carinicauda*, AEJ08191.1; *Atyopsis moluccensis*, CCF55379.1; *Caridina multidentate*, CCF55385.1; *Homarus americanus*, XP_042241812.1; *Panulirus japonicus*, BBO36752.1; *Trinorchestia longiramus*, KAF2367351.1. The blue shaded areas indicate the dee-sea hydrothermal vent shrimps.

conformational changes within Hc, are required. Throughout the adaptation process, these unique mutations were retained and could potentially provide advantages for the survival of deep-sea hydrothermal vent shrimps in extreme environments. Further functional experiments on mutation-induced changes in oxygen stoichiometry and innate immune activities are anticipated to provide insights into the implications of these unique mutations in *Hc* and elucidate the adaptation mechanisms of deep-sea hydrothermal vent shrimps.

Our analysis revealed intriguing patterns within the realm of positive selection underpinning deep-sea hydrothermal vent adaptation. Mutations within the active and binding sites suggested that these substitutions could potentially induce physiologically significant changes in the oxygenation properties of Hc. Although this study advances our understanding of the molecular adaptation of Hc in deep-sea hydrothermal vent shrimp, further studies involving functional experiments are required to provide deeper insights into the implications of these unique mutations.

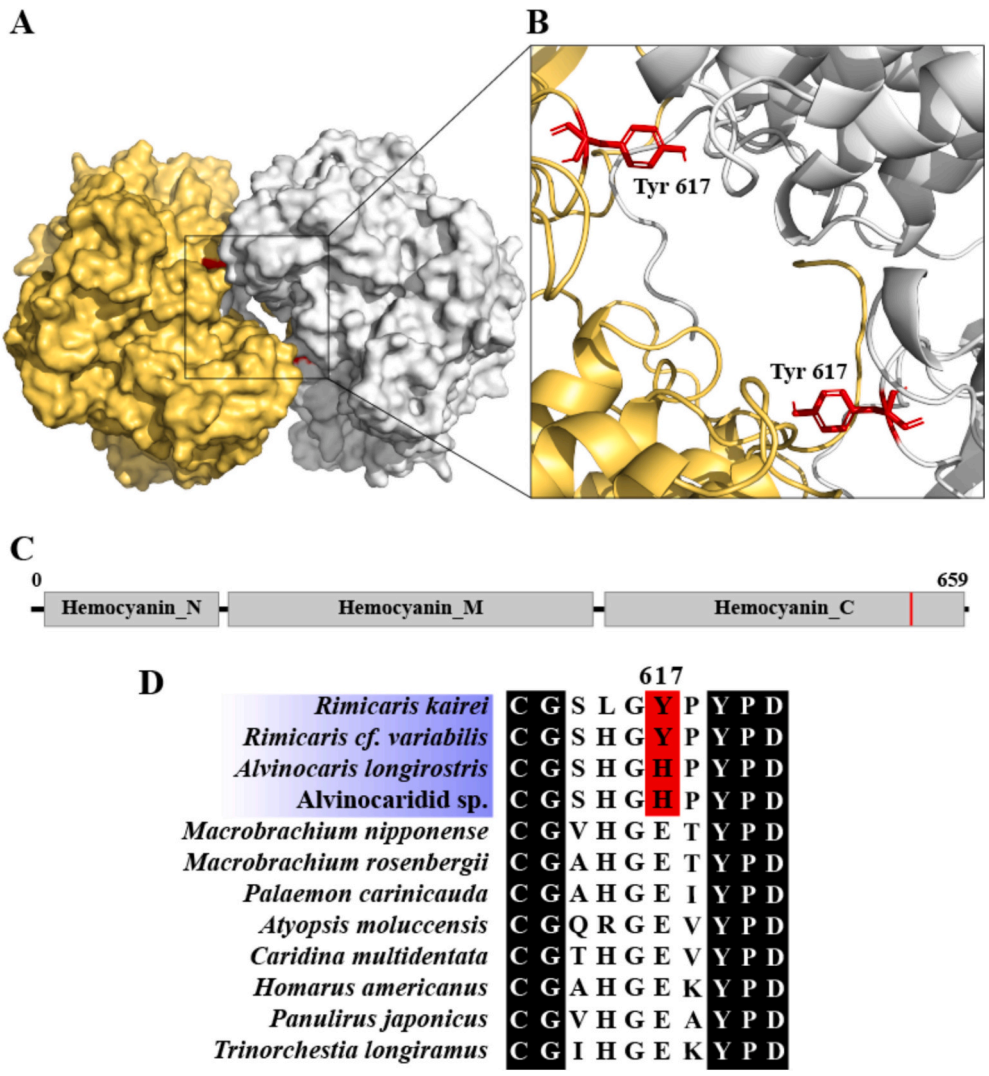

Fig. 4. (a) Three-dimensional structure of the α-type Hemocyanin (*RkaHc1*) dimer of *Rimicaris kairei* predicted using Cluspro 2.0 server. (a) The molecular surface of the dimer shows two *RkaHc1* (yellow and white). Positively selected sites of *RkaHc1* are indicated in red. (b) Ribbon diagram showing the close-up view of the interaction site. Positively selected residues (Tyr 617) are indicated in red. (c) Schematic representation of the domains of *RkaHc1*: Hemocyanin_N, Hemocyanin_M, and Hemocyanin_C. The three positively selected residues (red) detected within the binding site can be observed in the Hemocyanin_C domain. (d) Multiple sequence alignment (MSA) of the Hemocyanin_C domain from 12 decapods. The four deep-sea hydrothermal vent shrimps considered in this study are indicated in blue on the left side of the MSA. Mutation and highly conserved sites are indicated in red and black, respectively. Accession numbers: *Macrobrachium nipponense*, AEC46861.1; *Macrobrachium rosenbergii*, ALN67306.1; *Palaemon carinicauda*, AEJ08191.1; *Atyopsis moluccensis*, CCF55379.1; *Caridina multidentate*, CCF55385.1; *Homarus americanus*, XP_042241812.1; *Panulirus japonicus*, BBO36752.1; *Trinorchestia longiramus*, KAF2367351. The blue shaded areas indicate the dee-sea hydrothermal vent shrimps.

CRediT authorship contribution statement

Hyeongwoo Choi: Writing – review & editing, Writing – original draft, Visualization, Software, Investigation, Formal analysis, Data curation. **Ok-Hwan Yu:** Writing – review & editing, Resources. **Seong-il Eyun:** Writing – review & editing, Writing – original draft, Project administration, Funding acquisition, Conceptualization.

Ethics approval and consent to participate

Not applicable.

Declaration of competing interest

The authors declare that they have no known competing financial interests or personal relationships that could have appeared to influence the work reported in this paper.

Acknowledgments

This work was supported by the National Research Foundation of Korea (2022R1A2C4002058) and Korea Institute of Marine Science & Technology Promotion (RS-2021-KS211514, RS-2022-KS221676, and RS-2025-02215227) funded by the Ministry of Oceans and Fisheries.

Appendix A. Supplementary data

Supplementary data to this article can be found online at https://doi.org/10.1016/j.marpolbul.2025.117872.

Data availability

The raw sequence data generated in this study are openly available in the NCBI GenBank under accession number SRA (BioProject: PRJNA1012743). Furthermore, the sequences of four mitochondria

(OR570908-OR570911) and 15 *Hc* types (OR515021-OR515035) from four deep-shrimp species are available in the NCBI GenBank. All data sets used in this study are available at: http://eyunlab.cau.ac.kr/deepsea_shrimp.

References

Aweya, J.J., Zhuang, K., Liu, Y., Fan, J., Yao, D., Wang, F., Chen, X., Li, S., Ma, H., Zhang, Y., 2022. The ARM repeat domain of hemocyanin interacts with MKK4 to modulate antimicrobial peptides expression. iScience 25, 103958. https://doi.org/10.1016/j.isci.2022.103958.

Bak, H.J., Neuteboom, B., Jekel, P.A., Soeter, N.M., Vereijken, J.M., Beintema, J.J., 1986. Structure of arthropod hemocyanin. FEBS Lett. 204, 141–144. https://doi.org/10.1016/0014-5793(86)81402-8.

Bankevich, A., Nurk, S., Antipov, D., Gurevich, A.A., Dvorkin, M., Kulikov, A.S., Lesin, V. M., Nikolenko, S.I., Pham, S., Prjibelski, A.D., et al., 2012. SPAdes: a new genome assembly algorithm and its applications to single-cell sequencing. J. Comput. Biol. 19, 455–477. https://doi.org/10.1089/cmb.2012.0021.

Bendtsen J, Hansen JLS. Effects of global warming on hypoxia in the Baltic Sea–North Sea transition zone. 2013. Ecol. Model. 264:17–26. doi:https://doi.org/10.1016/j.ecolmodel.2012.06.018.

Bijlholt, M., van Bruggen, E.F., 1986. A model for the architecture of the hemocyanin from the arthropod *Squilla mantis* (Crustacea, Stomatopoda). Eur. J. Biochem. 155, 339–344. https://doi.org/10.1111/j.1432-1033.1986.tb09496.x.

Brouwer, M., Bonaventura, C., Bonaventura, J., 1978. Analysis of the effect of three different allosteric ligands on oxygen binding by hemocyanin of the shrimp, *Penaeus setiferus*. Biochemistry 17, 2148–2154. https://doi.org/10.1021/bi00604a019.

Burmester, T., 1999. Identification, molecular cloning, and phylogenetic analysis of a non-respiratory pseudo-hemocyanin of *Homarus americanus*. J. Biol. Chem. 274, 13217–13222. https://doi.org/10.1074/jbc.274.19.13217.

Burmester, T., 2001. Molecular evolution of the arthropod hemocyanin superfamily. Mol. Biol. Evol. 18, 184–195. https://doi.org/10.1093/oxfordjournals.molbev.a003792.

Burmester, T., 2002. Origin and evolution of arthropod hemocyanins and related proteins. J. Comp. Physiol. B 172, 95–107. https://doi.org/10.1007/s00360-001-0247-7.

Burmester, T., 2004. Evolutionary history and diversity of arthropod hemocyanins. Micron 35, 121–122. https://doi.org/10.1016/j.micron.2003.10.034.

Choi H, Nam J, Yang S, Eyun S. Highly contiguous genome assembly and gene annotation of the short-finned eel (*Anguilla bicolor pacifica*). 2024. Scientific Data. 11:952. doi: https://doi.org/10.1038/s41597-024-03817-9.

Choi, H., An, Y.K., Lee, C.J., Song, Cu, Kim, E.J., Lee, C.E., Cho, S.J., Eyun, S, 2025. Genome assembly, gene content, and plastic gene expression responses to salinity changes in the Brackishwater Clam (Corbicula japonica) from a dynamic estuarine environment. J. Hazard. Mater. 483, 136627. https://doi.org/10.1016/j.jhazmat.2024.136627.

Coates, C.J., Costa-Paiva, E.M., 2020. Multifunctional roles of hemocyanins. Subcell. Biochem. 94, 233–250. https://doi.org/10.1007/978-3-030-41769-7_9.

Decelle, J., Andersen, A.C., Hourdez, S., 2010. Morphological adaptations to chronic hypoxia in deep-sea decapod crustaceans from hydrothermal vents and cold seeps. Mar. Biol. 157, 1259–1269. https://doi.org/10.1007/s00227-010-1406-8.

Defur, P.L., Mangum, C., Reese, J.E., 1990. Respiratory responses of the blue crab *Callinectes sapidus* to long-term hypoxia. Biol. Bull. 178, 46–54. https://doi.org/10.2307/1541536.

Dillon, M.E., Wang, G., Huey, R.B., 2010. Global metabolic impacts of recent climate warming. Nature 467, 704–706. https://doi.org/10.1038/nature09407.

Fong JH, Marchler-Bauer A. Protein subfamily assignment using the conserved domain database. 2008. BMC research notes. 1:114. doi:https://doi.org/10.1186/1756-0500-1-114.

Gurevich, A., Saveliev, V., Vyahhi, N., Tesler, G., 2013. QUAST: quality assessment tool for genome assemblies. Bioinformatics 29, 1072–1075. https://doi.org/10.1093/bioinformatics/btt086.

Hourdez, S., Lallier, F.H., 2007. Adaptations to hypoxia in hydrothermal-vent and cold-seep invertebrates. Rev. Environ. Sci. Technol. 6, 143–159. https://doi.org/10.1007/978-1-4020-6285-8-19.

Hourdez, S., Weber, R.E., 2005. Molecular and functional adaptations in deep-sea hemoglobins. J. Inorg. Biochem. 99, 130–141. https://doi.org/10.1016/j.jinorgbio.2004.09.017.

Hourdez, S., Weber, R.E., Green, B.N., Kenney, J.M., Fisher, C.R., 2002. Respiratory adaptations in a deep-sea orbiniid polychaete from Gulf of Mexico brine pool NR-1: metabolic rates and hemoglobin structure/function relationships. J. Exp. Biol. 205, 1669–1681. https://doi.org/10.1242/jeb.205.11.1669.

Hui, M., Song, C., Liu, Y., Li, C., Cui, Z., 2017. Exploring the molecular basis of adaptive evolution in hydrothermal vent crab *Austinograea alayseae* by transcriptome analysis. PloS One 12, e0178417. https://doi.org/10.1371/journal.pone.0178417.

Jaenicke, E., Decker, H., Gebauer, W., Markl, J., Burmester, T., 1999. Identification, structure, and properties of hemocyanins from diplopod Myriapoda. J. Biol. Chem. 274, 29071–29074. https://doi.org/10.1074/jbc.274.41.29071.

Jiewkok, A., Tsukimura, B., Utarabhand, P., 2015. Purification and molecular cloning of Hemocyanin from *Fenneropenaeus Merguiensis* (De Man, 1888): response to *Vibrio harveyi* exposure. J. Crustac. Biol. 35, 659–669. https://doi.org/10.1163/1937240x-00002356.

Jumper, J., Evans, R., Pritzel, A., Green, T., Figurnov, M., Ronneberger, O., Tunyasuvunakool, K., Bates, R., Žídek, A., Potapenko, A., et al., 2021. Highly accurate protein structure prediction with AlphaFold. Nature 596, 583–589. https://doi.org/10.1038/s41586-021-03819-2.

Jung, H., Ventura, T., Chung, J.S., Kim, W.J., Nam, B.H., Kong, H.J., Kim, Y.O., Jeon, M. S., Eyun, S., 2020. Twelve quick steps for genome assembly and annotation in the classroom. PLoS Comput. Biol. 16, e1008325. https://doi.org/10.1371/journal.pcbi.1008325.

Kalyaanamoorthy, S., Minh, B.Q., Wong, T.K.F., von Haeseler, A., Jermiin, L.S., 2017. ModelFinder: fast model selection for accurate phylogenetic estimates. Nat. Methods 14, 587–589. https://doi.org/10.1038/nmeth.4285.

Katoh, K., Misawa, K., Kuma, K.I., Miyata, T., 2002. MAFFT: a novel method for rapid multiple sequence alignment based on fast fourier transform. Nucleic Acids Res. 30, 3059–3066. https://doi.org/10.1093/nar/gkf436.

Kozakov, D., Hall, D.R., Xia, B., Porter, K.A., Padhorny, D., Yueh, C., Beglov, D., Vajda, S., 2017. The ClusPro web server for protein-protein docking. Nat. Protoc. 12, 255–278. https://doi.org/10.1038/nprot.2016.169.

Kozlov, A.M., Darriba, D., Flouri, T., Morel, B., Stamatakis, A., 2019. RAxML-NG: a fast, scalable and user-friendly tool for maximum likelihood phylogenetic inference. Bioinformatics 35, 4453–4455. https://doi.org/10.1093/bioinformatics/btz305.

Krzywinski, M., Schein, J., Birol, I., Connors, J., Gascoyne, R., Horsman, D., Jones, S.J., Marra, M.A., 2009. Circos: an information aesthetic for comparative genomics. Genome Res. 19, 1639–1645. https://doi.org/10.1101/gr.092759.109.

Kusche, K., Hembach, A., Hagner-Holler, S., Gebauer, W., Burmester, T., 2003. Complete subunit sequences, structure and evolution of the 6×6-mer hemocyanin from the common house centipede, *Scutigera coleoptrata*. Eur. J. Biochem. 270, 2860–2868. https://doi.org/10.1046/j.1432-1033.2003.03664.x.

Lallier, F.H., Truchot, J.P., 1997. Hemocyanin oxygen-binding properties of a deep-sea hydrothermal vent shrimp: evidence for a novel cofactor. J. Exp. Zool. 277, 357–364. https://doi.org/10.1002/(SICI)1097-010X(19970401)277:5<357::AID-JEZ1>3.0.CO;2-O.

Lanfear, R., Frandsen, P.B., Wright, A.M., Senfeld, T., Calcott, B., 2016. PartitionFinder 2: new methods for selecting partitioned models of evolution for molecular and morphological phylogenetic analyses. Mol. Biol. Evol. 34, 772–773. https://doi.org/10.1093/molbev/msw260.

Le Layec V, Hourdez S. Oxygen consumption rates in deep-sea hydrothermal vent scale worms: Effect of life-style, oxygen concentration, and temperature sensitivity. 2021. Deep Sea Research Part I: Oceanographic Research Papers. 172:103531. doi:https://doi.org/10.1016/j.dsr.2021.103531.

Li, J., Zhao, M., Zhang, X., Zheng, Z., Yao, D., Yang, S., Chen, T., Zhang, Y., Aweya, J.J., 2024. The evolutionary adaptation of shrimp hemocyanin subtypes and the consequences on their structure and functions. Fish Shellfish Immunol. 145, 109347. https://doi.org/10.1016/j.fsi.2023.109347.

Liang, H., Zhou, W., Landweber, L.F., 2006. SWAKK: a web server for detecting positive selection in proteins using a sliding window substitution rate analysis. Nucleic Acids Res. 34, W382–W384. https://doi.org/10.1093/nar/gkl272.

Liu, M., Zhang, Y., Shi, K., Zhu, G., Wu, Z., Liu, M., Zhang, Y., 2019. Thermal stratification dynamics in a large and deep subtropical reservoir revealed by high-frequency buoy data. Sci. Total Environ. 651, 614–624. https://doi.org/10.1016/j.scitotenv.2018.09.215.

Mangum, C.P., 1994. Subunit composition of hemocyanins of *Callinectes sapidus*: phenotypes from naturally hypoxic waters and isolated oligomers. Comparative Biochemistry and Physiology Part B: Comparative Biochemistry. 108, 537–541. https://doi.org/10.1016/0305-0491(94)90107-4.

Markl, J., 1986. Evolution and function of structurally diverse subunits in the respiratory protein hemocyanin from arthropods. Biol. Bull. 171, 90–115. https://doi.org/10.2307/1541909.

Markl, J., 2013. Evolution of molluscan hemocyanin structures. Biochimica et Biophysica Acta (BBA). 1834, 1840–1852. https://doi.org/10.1016/j.bbapap.2013.02.020.

Martin, M., 2011. Cutadapt removes adapter sequences from high-throughput sequencing reads. EMBnet J. 17, 10–12. https://doi.org/10.14806/ej.17.1.200.

Matear, R.J., Hirst, A.C., 2003. Long-term changes in dissolved oxygen concentrations in the ocean caused by protracted global warming. Global Biogeochem. Cycles 17. https://doi.org/10.1029/2002GB001997.

Meng G, Li Y, Yang C, Liu S. MitoZ: a toolkit for animal mitochondrial genome assembly, annotation and visualization. 2019. Nucleic Acids Research. 47:e63. doi:https://doi.org/10.1093/nar/gkz173.

Miller, K.I., Eldred, N.W., Arisaka, F., Van Holde, K.E., 1977. Structure and function of hemocyanin from thalassinid shrimp. J. Comp. Physiol. 115, 171–184. https://doi.org/10.1007/BF00692528.

Minh, B.Q., Schmidt, H.A., Chernomor, O., Schrempf, D., Woodhams, M.D., von Haeseler, A., Lanfear, R., 2020. IQ-TREE 2: new models and efficient methods for phylogenetic inference in the genomic era. Mol. Biol. Evol. 37, 1530–1534. https://doi.org/10.1093/molbev/msaa015.

Pal S, Tiwari A, Sharma K, Sharma SK. Does conserved domain *SOD1* mutation has any role in ALS severity and therapeutic outcome? 2020. BMC Neuroscience. 21:42. doi: https://doi.org/10.1186/s12868-020-00591-3.

Rambaut, A., Grass, N.C., 1997. Seq-Gen: an application for the Monte Carlo simulation of DNA sequence evolution along phylogenetic trees. Bioinformatics 13, 235–238. https://doi.org/10.1093/bioinformatics/13.3.235.

Ronquist, F., Teslenko, M., van der Mark, P., Ayres, D.L., Darling, A., Höhna, S., Larget, B., Liu, L., Suchard, M.A., Huelsenbeck, J.P., 2012. MrBayes 3.2: efficient Bayesian phylogenetic inference and model choice across a large model space. Syst. Biol. 61, 539–542. https://doi.org/10.1093/sysbio/sys029.

Schrödinger, L., DeLano, W., 2020. PyMOL. Version 2.4.0.

Schultz, J., Copley, R.R., Doerks, T., Ponting, C.P., Bork, P., 2000. SMART: a web-based tool for the study of genetically mobile domains. Nucleic Acids Res. 28, 231–234. https://doi.org/10.1093/nar/28.1.231.

Sellos, D., Lemoine, S., Van Wormhoudt, A., 1997. Molecular cloning of hemocyanin cDNA from *Penaeus vannamei* (Crustacea, Decapoda): structure, evolution and physiological aspects. FEBS Lett. 407, 153–158. https://doi.org/10.1016/S0014-5793(97)00350-5.

Simão, F.A., Waterhouse, R.M., Ioannidis, P., Kriventseva, E.V., Zdobnov, E.M., 2015. BUSCO: assessing genome assembly and annotation completeness with single-copy orthologs. Bioinformatics 31, 3210–3212. https://doi.org/10.1093/bioinformatics/btv351.

Stanke, M., Morgenstern, B., 2005. AUGUSTUS: a web server for gene prediction in eukaryotes that allows user-defined constraints. Nucleic Acids Res. 33, W465–W467. https://doi.org/10.1093/nar/gki458.

Stöcker, W., Raeder, U., Bijlholt, M.M.C., Wichertjes, T., van Bruggen, E.F., Markl, J., 1988. The quaternary structure of four crustacean two-hexameric hemocyanins: immunocorrelation, stoichiometry, reassembly and topology of individual subunits. J. Comp. Physiol. B 158, 271–289. https://doi.org/10.1007/BF00695326.

Sun, S., Chen, L., Qin, J., Ye, J., Qin, C., Jiang, H., Li, E., 2012. Molecular cloning, characterization and mRNA expression of copper-binding protein hemocyanin subunit in Chinese mitten crab, *Eriocheir sinensis*. Fish Shellfish Immunol. 33, 1222–1228. https://doi.org/10.1016/j.fsi.2012.09.023.

Suyama, M., Torrents, D., Bork, P., 2006. PAL2NAL: robust conversion of protein sequence alignments into the corresponding codon alignments. Nucleic Acids Res. 34, W609–W612. https://doi.org/10.1093/nar/gkl315.

Todorovska E, Ivanov M, Radkova M, Dolashki A, Dolashka P. Molecular cloning, structure and phylogenetic analysis of a hemocyanin subunit from the black sea crustacean *Eriphia verrucosa* (Crustacea, Malacostraca). 2021. Genes. 12:93. doi: https://doi.org/10.3390/genes12010093.

Van Dover, C.L., 2000. The Ecology of Deep-Sea Hydrothermal Vents. Princeton University Press.

Van Holde, K.E., Miller, K.I., 1995. Hemocyanins. Adv. Protein Chem. 47, 1–81.

Wu, R.S.S., 2002. Hypoxia: from molecular responses to ecosystem responses. Mar. Pollut. Bull. 45, 35–45. https://doi.org/10.1016/S0025-326X(02)00061-9.

Yang, Z., 2007. PAML 4: phylogenetic analysis by maximum likelihood. Mol. Biol. Evol. 24, 1586–1591. https://doi.org/10.1093/molbev/msm088.

Zhang, Y., Yan, F., Hu, Z., Zhao, X., Min, S., Du, Z., Zhao, S., Ye, X., Li, Y., 2009. Hemocyanin from shrimp *Litopenaeus vannamei* shows hemolytic activity. Fish Shellfish Immunol. 27, 330–335. https://doi.org/10.1016/j.fsi.2009.05.017.

Zhao, L., Sun, T., Pei, J., Ouyang, Q., 2015. Mutation-induced protein interaction kinetics changes affect apoptotic network dynamic properties and facilitate oncogenesis. Proc. Natl. Acad. Sci. USA 112, E4046–E4054. https://doi.org/10.1073/pnas.1502126112.

Zhao, M., Aweya, J.J., Feng, Q., Zheng, Z., Yao, D., Zhao, Y., Chen, X., Zhang, Y., 2022. Ammonia stress affects the structure and function of hemocyanin in *Penaeus vannamei*. Ecotoxicol. Environ. Saf. 241, 113827. https://doi.org/10.1016/j.ecoenv.2022.113827.